Isoforms confer characteristic force generation and mechanosensation by myosin II filaments

Samantha Stam[1,2], Jon Alberts[3], Margaret L. Gardel[2,4], Edwin Munro[2,5]

[1]Biophysical Sciences Graduate Program, [2]Institute for Biophysical Dynamics,
[3]University of Washington, Friday Harbor, Washington
[4]Physics Department & James Franck Institute,
[5]Department of Molecular Genetics and Cell Biology
University of Chicago, Chicago, IL 60637

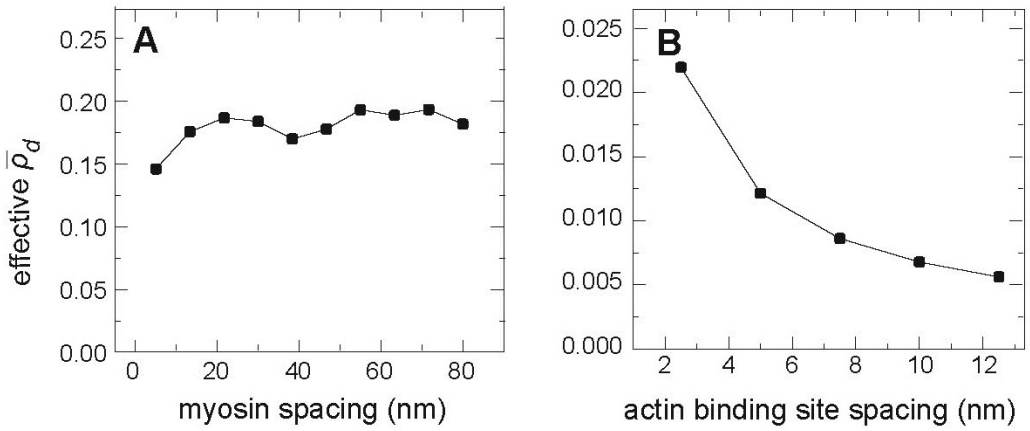

Figure S1. Dependence of effective duty ratio (ρ_d) on the spacing of myosin motors and actin filament binding sites in simulated gliding assays. (A) Dependence of ρ_d on motor spacing using parameters for non-muscle myosin IIB from Table 2 and N_{heads} = 50. The spacing that we used in our simulations was 5 nm, which is smaller than the experimentally estimated value of 40 nm reported in reference 24. However, varying this value from 5 to 80 had little effect on the average duty ratio even for these relatively high duty ratio motors. (B) Dependence of ρ_d on the spacing of filament binding sites for motors approximating skeletal muscle myosin II with N_{heads} = 50. The spacing that we used, 2.7 nm, differed from the experimentally measured value of 5.5 nm reported in reference 43. However, higher values lead to a reduction in average duty ratio due to binding-site limited attachment of motors even for the relatively low-duty ratio skeletal muscle parameters. The value that we used yields an appropriate duty ratio. Each data point is the average of 1000 values over a 100 s simulation.

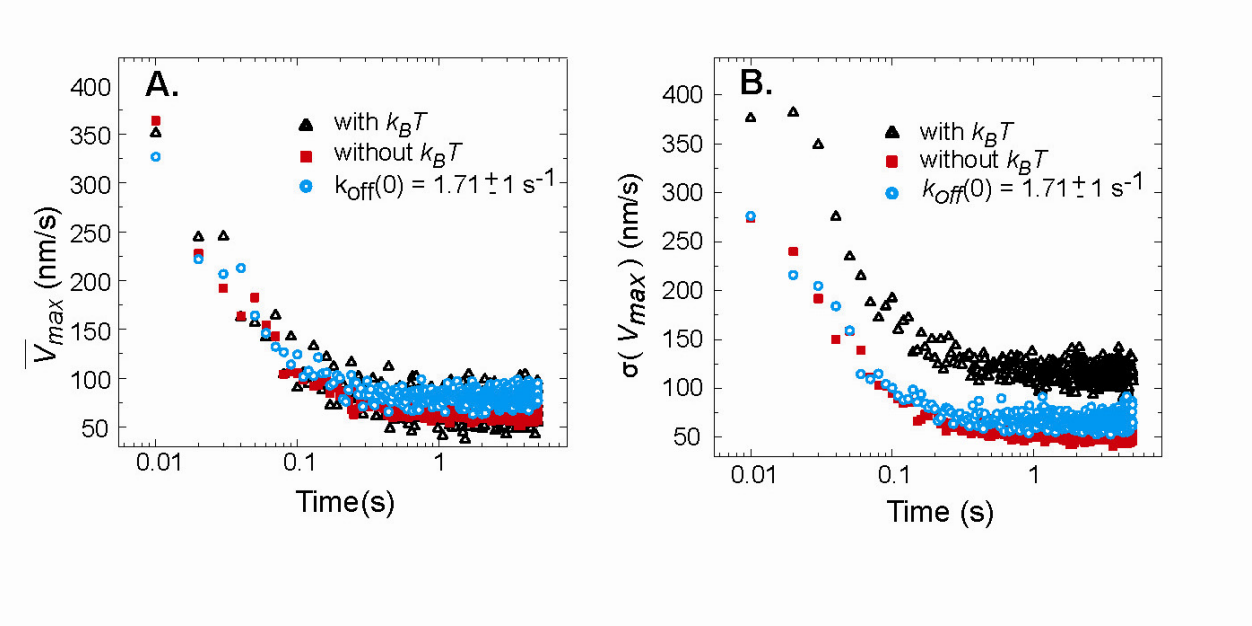

Figure S2. Rapid approach to steady state from an initially unbound condition during simulated unloaded gliding. (A) Average timecourse of unloaded gliding velocity with or without thermal noise or random variation in the value of $k_{off}(0)$ across the ensemble. (B) Standard deviations corresponding to the averages in (A). Each data point is the average or standard deviation from 100 individual simulations. Parameter choices: NM IIA parameters from Table 2 and N_{heads} = 500.

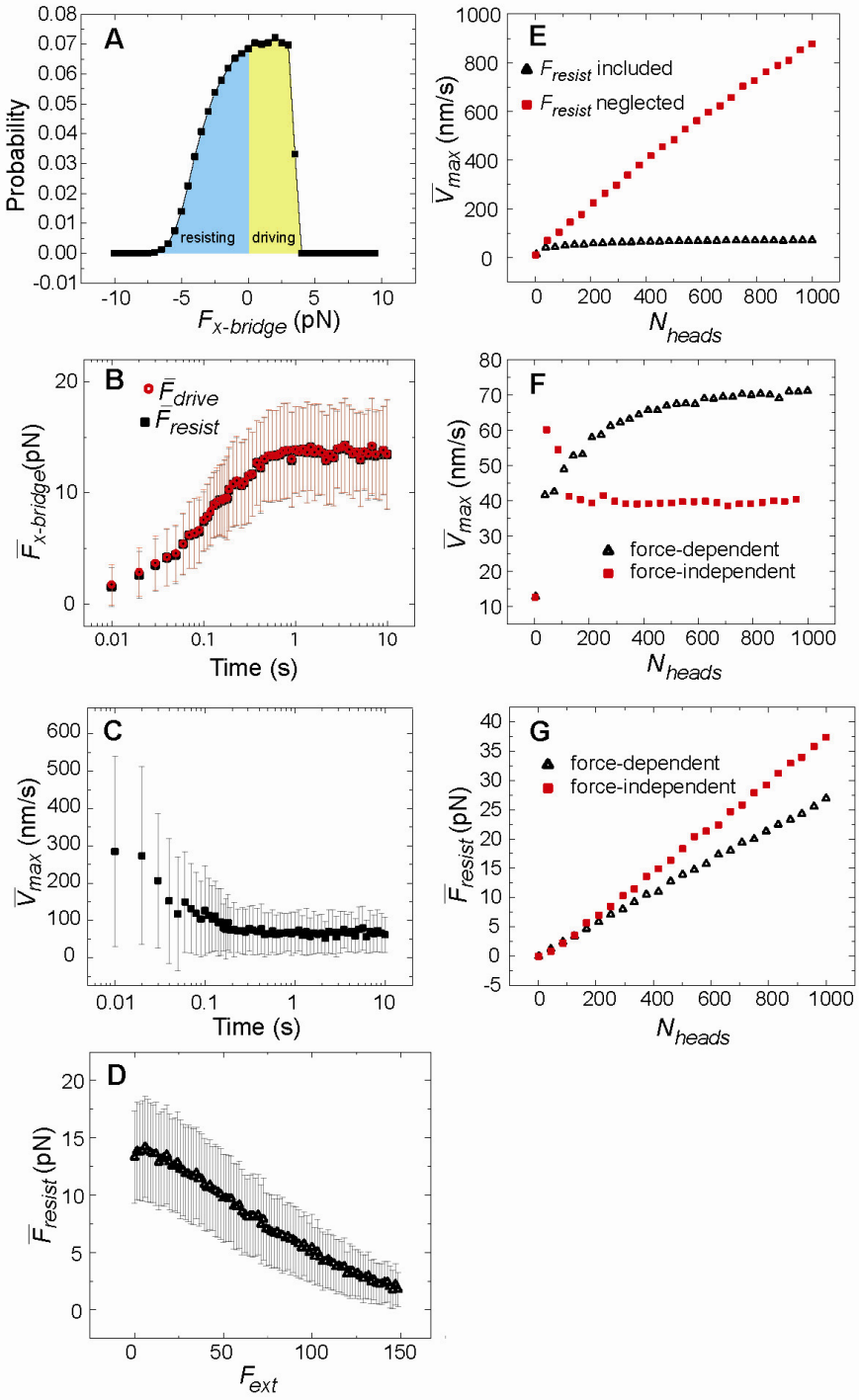

Figure S3. Effective internal resistance of elastic crossbridges limits gliding velocities. (A) Distribution of positive (driving) and negative (resisting) forces on individual myosin cross-bridges during steady state gliding of an unloaded actin filament. (B) Accumulation of driving and resisting forces from an initial state in which all motors are unbound. (C) Evolution of the unloaded gliding velocity, V_{max}, from the same initial condition as in (B). (D) The resisting force from negatively strained crossbridges decreases with F_{ext}. (E) Comparison of average unloaded gliding velocities in simulations where resisting forces from negatively strained crossbridges are either included or neglected in the equation of motion. (F) Comparison of average unloaded gliding velocities with force-dependent or independent k_{off}. (G) The resisting force from negatively strained crossbridges decreases with use of force-dependent kinetics. Panels (A) and (D)-(G) display data from 1000 samples averaged over 100 s of simulation time. Panels (B) and (C) display average data over 100 independent runs. Error bars indicate standard deviation. Parameter choices: (A-G) NM IIA parameters from Table 2, (A-D) N_{heads} = 500.

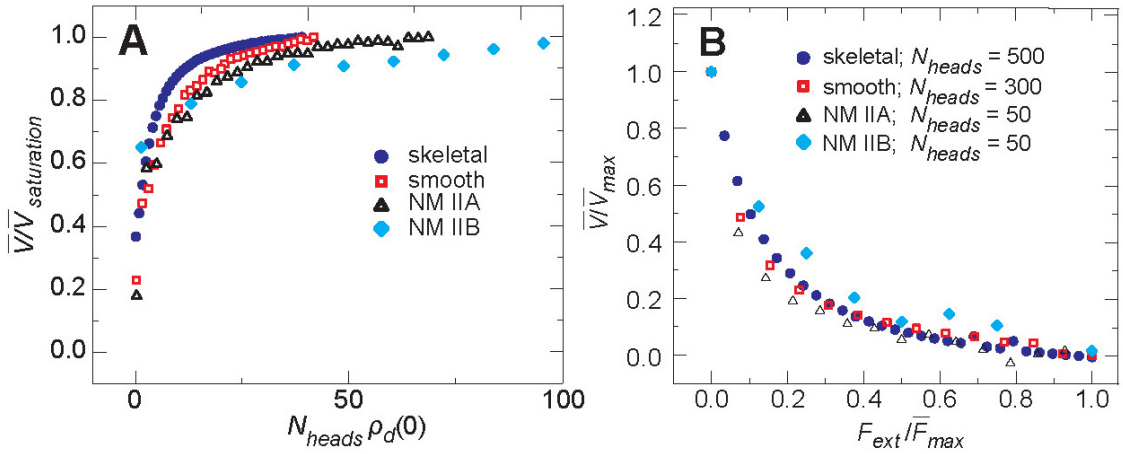

Figure S4. Scaling of unloaded gliding velocity vs. motor density and force vs. velocity curves. (A) Isoform-specific plots of gliding velocity vs. motor density from Fig. 1C collapse when the horizontal axis is scaled by plateau velocity at large N_{heads} and the vertical axis is scaled by the unloaded motor duty ratio. (B) Isoform-specific plots of force vs. velocity from Fig. 1D collapse when the horizontal and vertical axes are scaled respectively by $\bar{F}_{max}$ and $\bar{V}_{max}$. Each data point is the average of 10^7 samples over 100 s of simulation time.

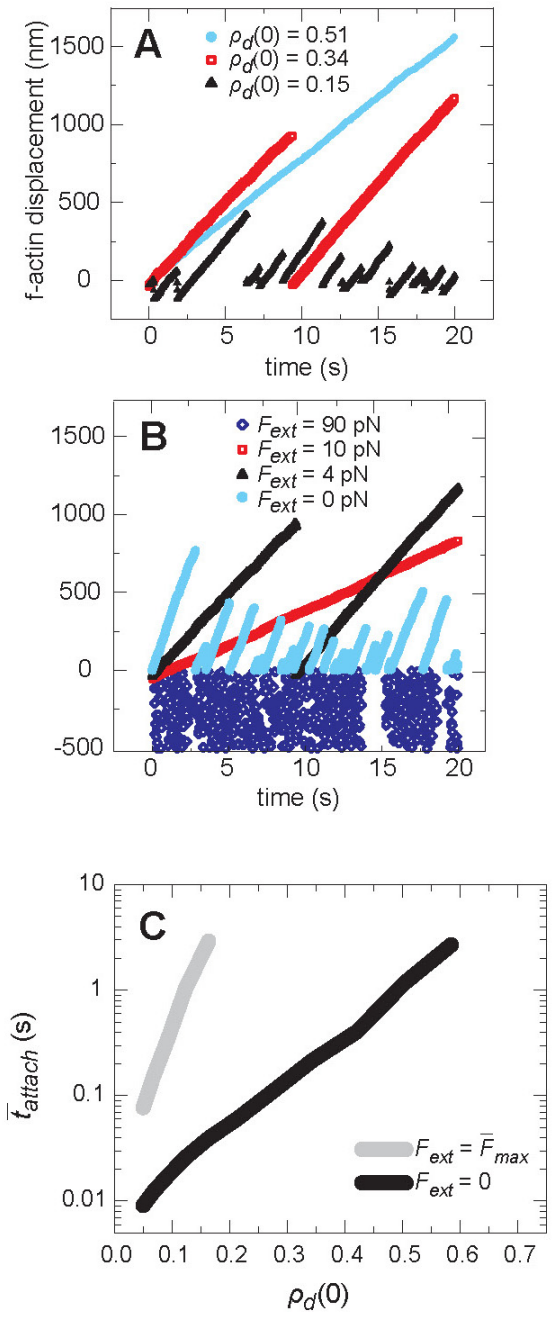

Figure S5: Dependence of motor cluster processivity on unloaded duty ratio $\rho_d(0)$ and external load F_{ext}. (A) and (B) Simulated actin filament trajectories for different values of $\rho_d(0)$ (A) or F_{ext} (B). (C) Dependence of mean attachment time ($\bar{t}_{attach}$) on duty ratio $\rho_d(0)$ is exponential and significantly sharper for stalled vs unloaded conditions. Parameter values in (A-C): k_{on} = 10 s^{-1}, N_{heads} = 15, (A): F_{ext} = 4 pN, and (B): $\rho_d(0)$ = 0.34 ($k_{off}(0)$ = 19 s^{-1}). In (C), averages were taken over 100 s of simulation time.

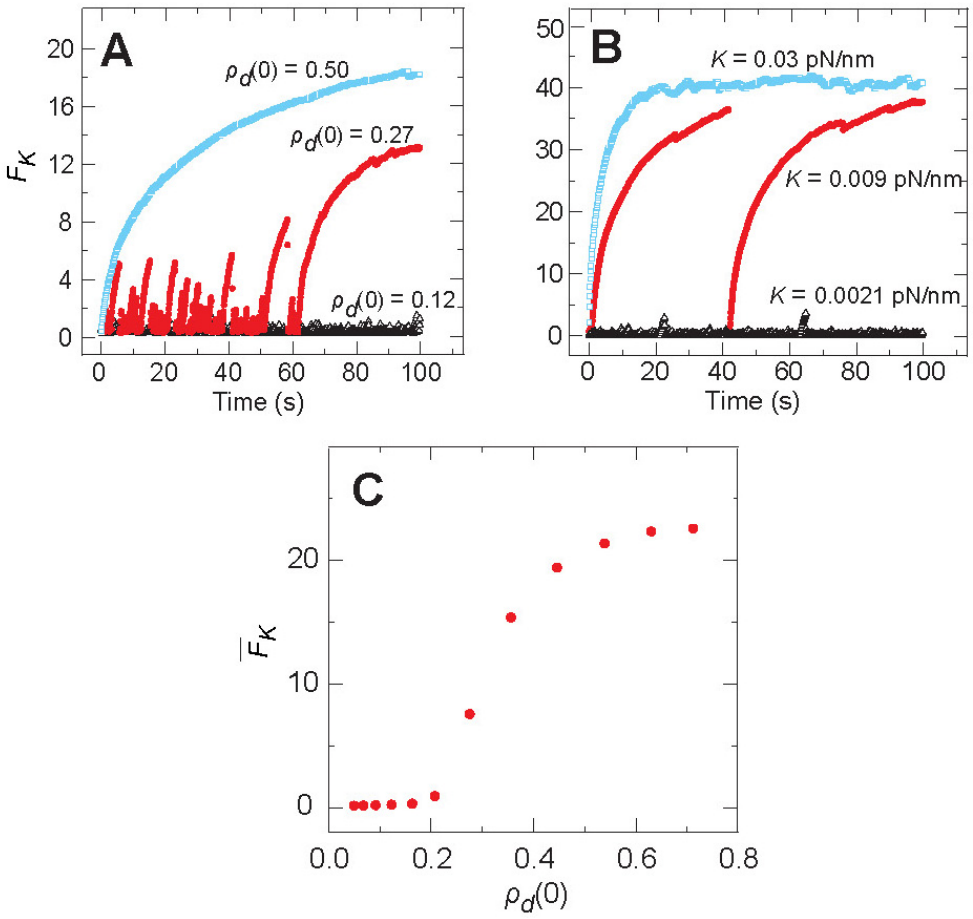

Figure S6: Dependence of force buildup on unloaded duty ratio $\rho_d(0)$ and environmental stiffness K. (A) and (B) The force F_K generated by the motor cluster against an external elastic load over time for different values of $\rho_d(0)$ (A) or K (B). (C) Average value of F_K measured as a function of $\rho_d(0)$. Each point is the average of 10000 values from 10 independent simulations of 100 s. Parameter values in (A): k_{on} = 10 s^{-1}, N_{heads} = 10, K = 0.02 pN/nm, (B): $\rho_d(0)$ = 0.05 (k_{on} = 10 s^{-1}, $k_{off}(0)$ = 191), N_{heads} = 74, and (C): k_{on} = 10 s^{-1}, N_{heads} = 10, K = 0.02 pN/nm.

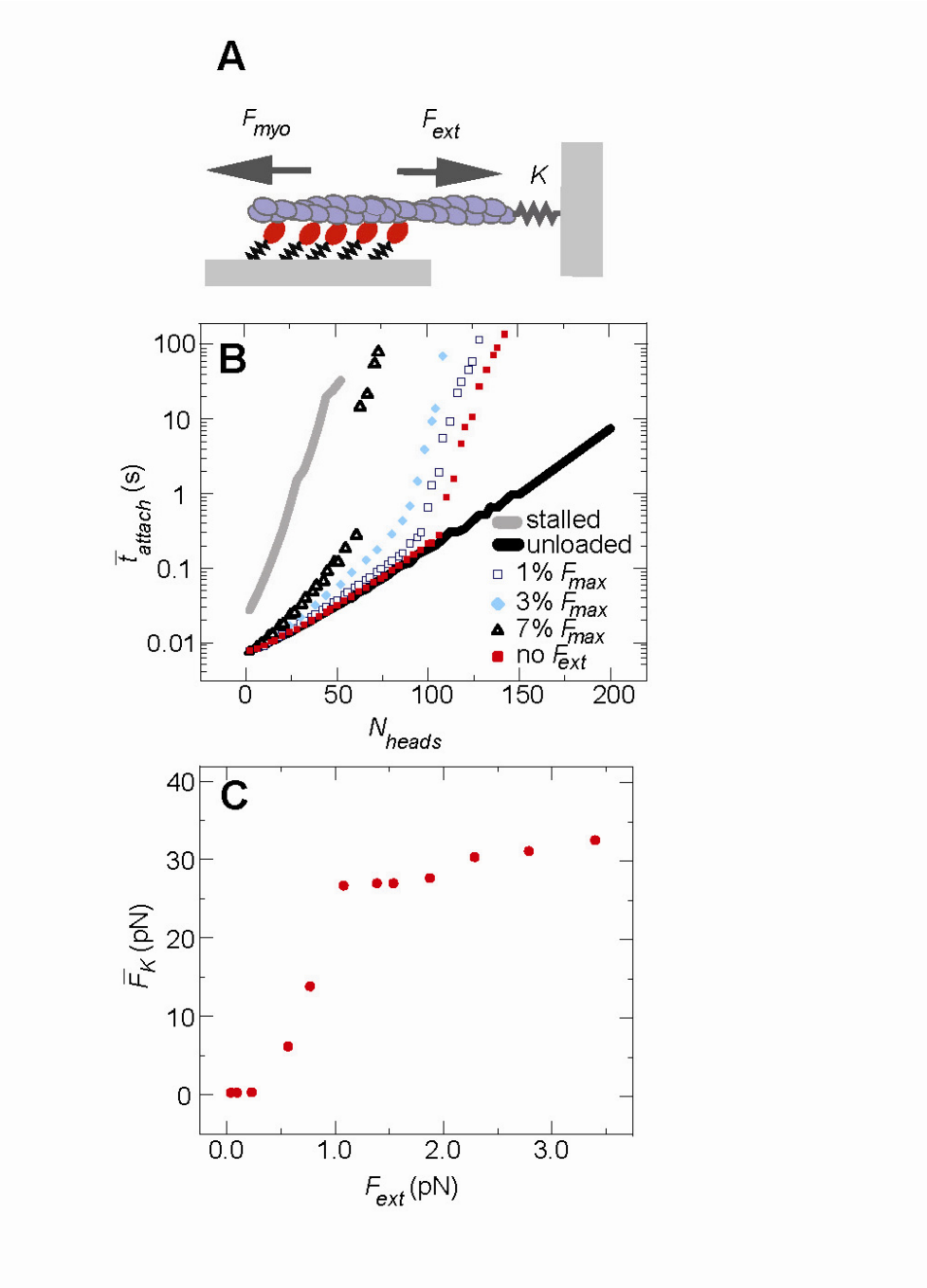

Figure S7: A small constant force superimposed on a linear load can trigger processive force generation. (A) Schematic of myosin motors building force on a linear spring against a small opposing force F_{ext}. (B) Dependence of the average attached time of the actin filament on N_{heads} for different values of F_{ext}. (C) Increase in the mean force generated against the elastic spring with increasing values of F_{ext}. Parameter values in (B): $\rho_d(0) = 0.05$ ($k_{on} = 10$ s^{-1} and $k_{off}(0) = 191$ s^{-1}), $K = 0.0006$ pN/nm (C): $\rho_d(0) = 0.05$ ($k_{on} = 10$ s^{-1} and $k_{off}(0) = 191$ s^{-1}), $K = 0.0006$ pN/nm, $N_{heads} = 100$. Averages were taken over 15 simulations of 1000 s.

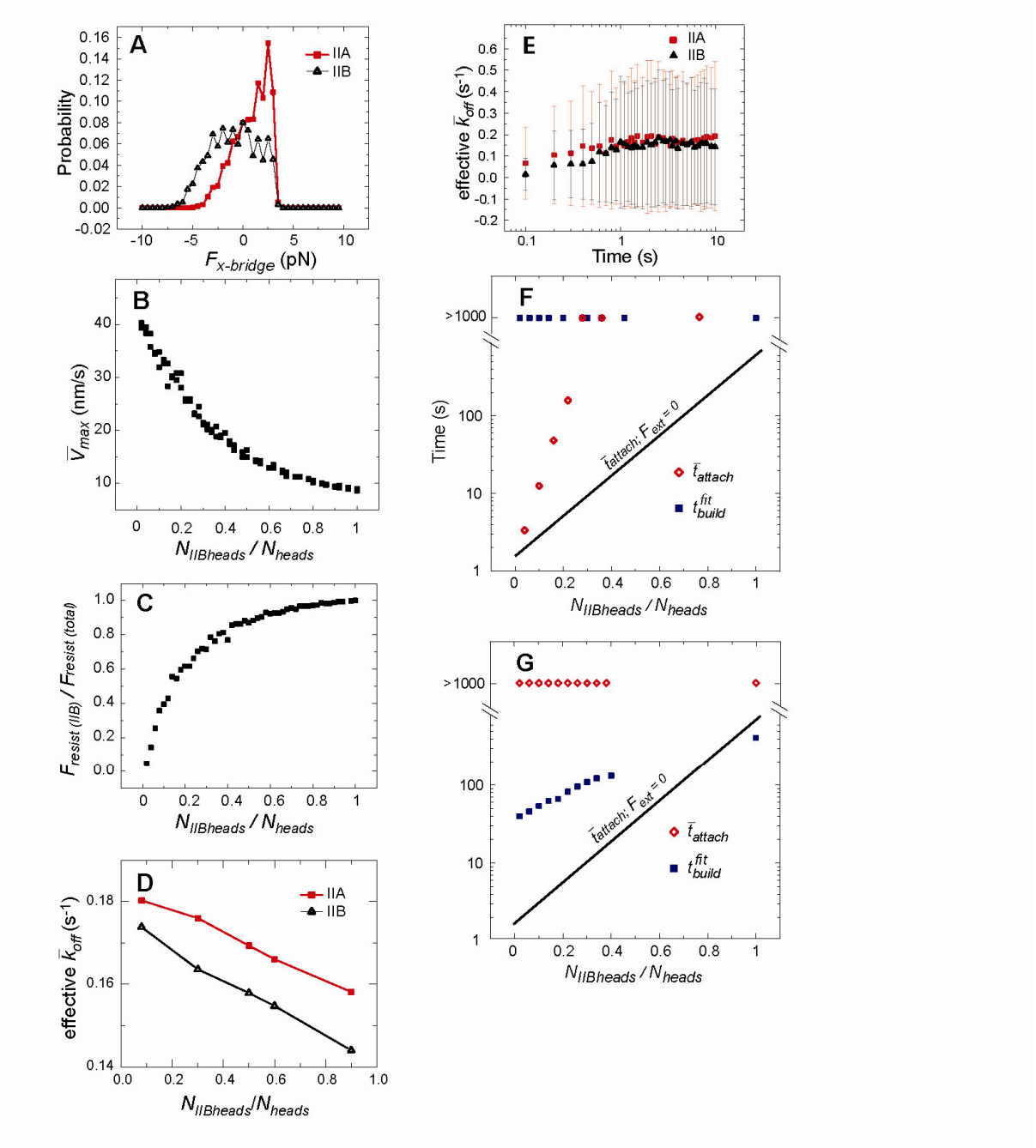

Figure S8: Coassembly of non-muscle myosin IIA and IIB (A) During unloaded gliding, isoforms show different distribution of crossbridge forces in mixed filament where $N_{IIAheads} = N_{IIBheads} = 25$. (B) Unloaded velocity decreases with increasing fraction of NM IIB. (C) Fraction of the total resistive forces sustained by NM IIB motors in (B). (D) Increasing the fraction of NM IIB decreases the measured cycling rate, or effective $\bar{k}_{off}$. (E) The effective $\bar{k}_{off}$ where $N_{IIAheads} = N_{IIBheads} = 25$ reaches a steady state on a similar timescale as velocities or forces in Fig. S2, S3B, and S3C. (F) and (G) Average t_{attach} and t_{build} on elastic load with $K = 0.004$ pN/nm (F) and $K = 0.4$ pN/nm (G). In all panels, the total $N_{heads} = 50$. In (A)-(C), 1000 data points were averaged over 100 s of simulation time. In (D), the effective k_{off} was averaged over 200 40 s simulations while (E) is the average of 200 10 s simulations. In (F) and (G), data points for $\bar{t}_{\text{attach}}$ are average values over 15 simulations of 1000 s while t_{build}^{fit} was calculated using a fit to the scaling relationship in Fig 4. Error bars represent standard deviation.

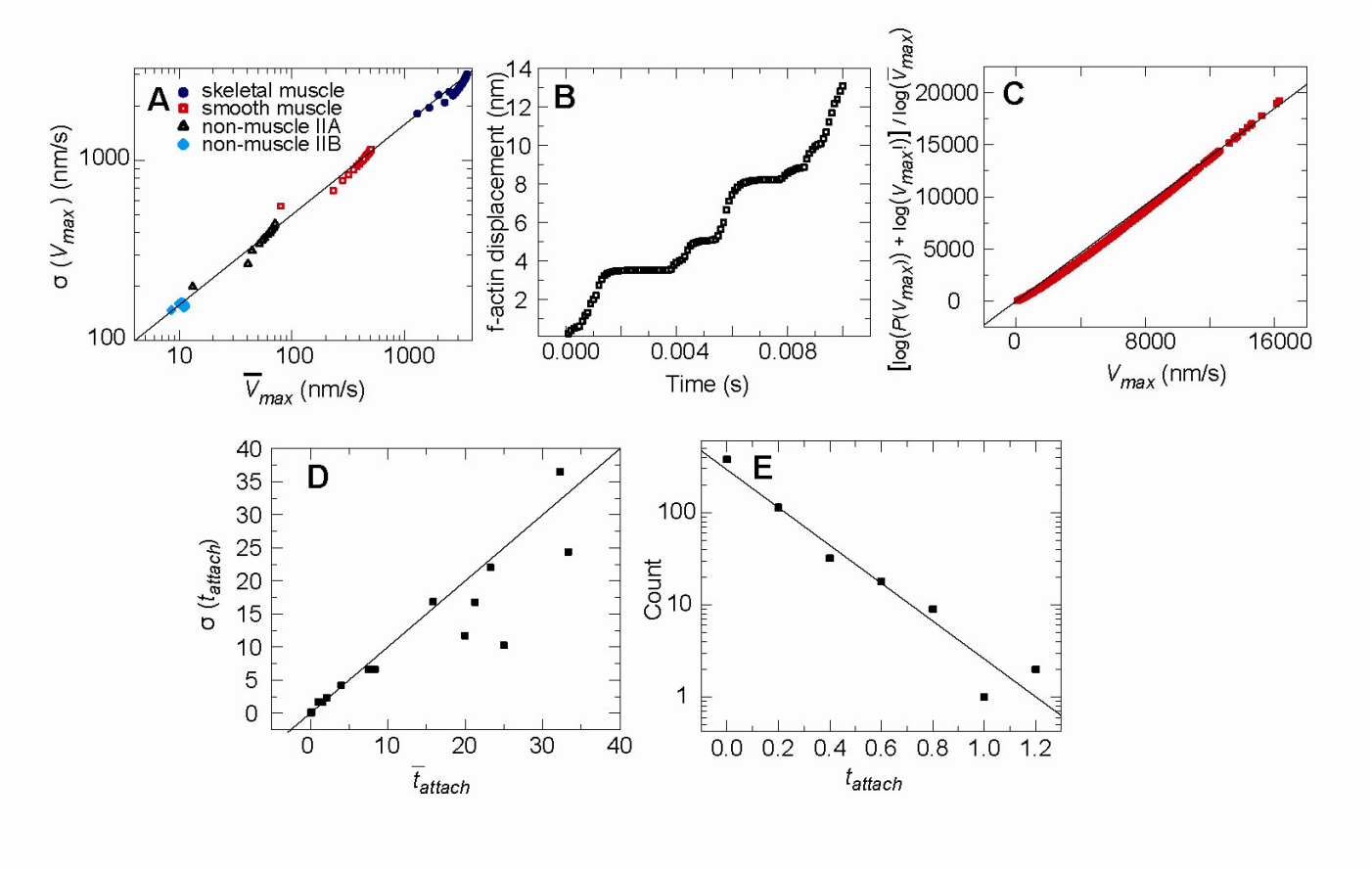

Fig. S9: Velocity and t_{attach} with constant F_{ext} are Poisson distributed. (A) The standard deviation of V_{max} at constant F_{ext} in Fig. 1C approximately scales as the square root of the average, $\bar{V}_{max}$, which is consistent with a Poisson process where V_{max} is proportional to motor steps per unit time. The solid line has a slope of 1/2 for reference. (B) Saltatory motion of actin at high time resolution occurs due to biochemical transitions and explains Poisson behavior. (C) The logarithm of the distribution of the velocities, P(V_{max}), shifted by the logarithm of the factorial of V_{max} and scaled by the logarithm of the average, $\bar{V}_{max}$. If Poisson statistics hold for actin gliding, this plot should be a line with a slope of 1. A least-squares fit indicates that a line with slope 1.12 fits with R^2 = 0.99. (D) The standard deviation of t_{attach} in Fig. 2B approximately scales with the average of t_{attach}, which is consistent with detachment being a Poisson process. The solid line shown is y = x. (E) The distribution of t_{attach}. This function should exponentially decay if detachment is in fact a Poisson process. A least squares fit of an exponential function shown approximates the data with R^2 = 0.94. Parameter values: (B)-(E) k_{on} =10, $k_{off}(0)$ = 191, F_{ext} = 0 and (B), (C), (E) N_{heads} = 100. Velocities in (A) and (C) are averages of 10^7 data points collected for 100 s of simulation time. Attachment times in (D) and (E) were averaged over 200 s simulations.

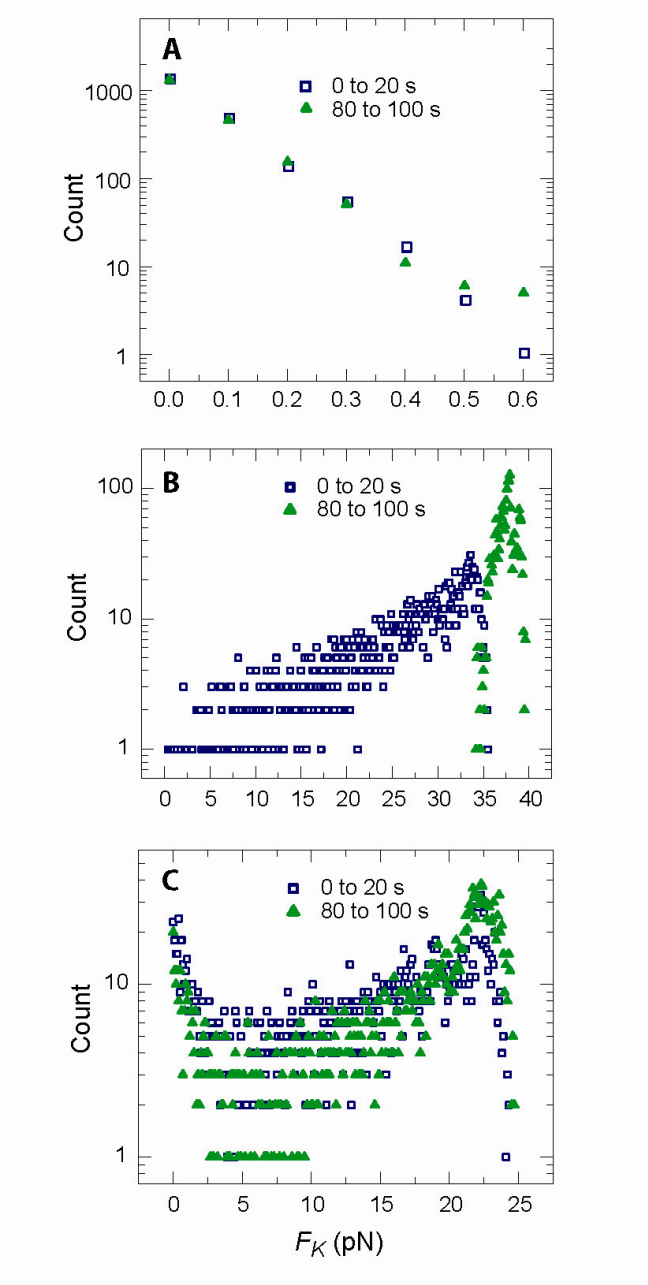

Figure S10: Distributions of forces generated by myosin motors during force buildup against an elastic load for different values of N_{heads}, corresponding to the mean values shown in Figure 3C. (A) For N_{heads} = 10, where minimal force is built, forces are exponentially distributed consistent with Fig. S9E. (B) At N_{heads} = 70, where the mean force approaches the maximum (stall) force, an initially broad distribution during force buildup collapses to a narrower distribution when filaments reach their stall force. (C) For the intermediate value of N_{heads} = 50, centered on the transition from low to high force, the distribution contains contains peaks both at the stall force and at low force. We observed the same distribution even at long times indicating that some filaments do not switch over to processive force buildup. In all panels, the force magnitude was sampled 10000 times over the course of ten 100 s simulations.